Article

Cell Chemical Biology

Differential effects of modified batrachotoxins on voltage-gated sodium channel fast and slow inactivation

Graphical abstract

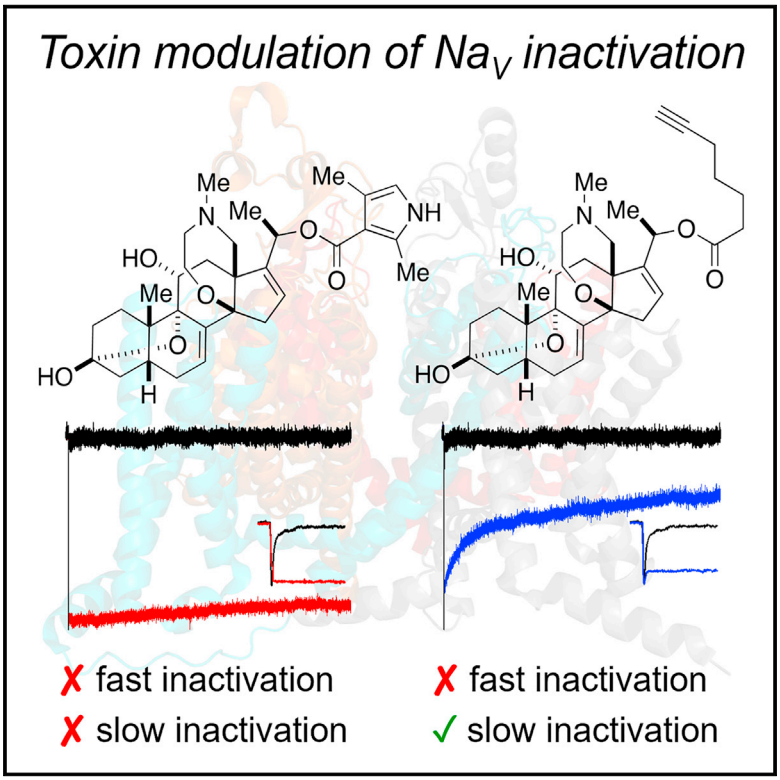

Highlights

- BTX and C20-ester derivatives modulate gating of sodium channel subtypes
- BTX hyperpolarizes voltage of activation and inhibits both fast and slow inactivation
- A BTX C20-ester differentiates fast and slow inactivation, only blocking the former

Authors

Tim M.G. MacKenzie, Fayal Abderemane-Ali, Catherine E. Garrison, Daniel L. Minor, Jr., J. Du Bois

Correspondence

jdubois@stanford.edu (J.D.), daniel.minor@ucsf.edu (D.L.M.)

In brief

BTX, an acute poison, acts as a potent allosteric regulator of Na_Vs. Structure-function analysis of BTX and three BTX C20-ester derivatives reveals unexpected differences in activity. One compound, BTX-yne, blocks fast but not slow inactivation of ion conduction and is thus distinguished from the others.

MacKenzie et al., 2022, Cell Chemical Biology *29*, 1–10
April 21, 2022
https://doi.org/10.1016/j.chembiol.2021.12.003

CellPress

Cell Chemical Biology

CellPress

Article

Differential effects of modified batrachotoxins on voltage-gated sodium channel fast and slow inactivation

Tim M.G. MacKenzie,[1,7] Fayal Abderemane-Ali,[2,7] Catherine E. Garrison,[1,7] Daniel L. Minor, Jr.,[2,3,4,5,6,*] and J. Du Bois[1,8,9,*]
[1]Department of Chemistry, Stanford University, 337 Campus Drive, Stanford, CA 94305, USA
[2]Cardiovascular Research Institute, University of California, San Francisco, Box 3122, 555 Mission Bay Boulevard South, Rm. 452Z, San Francisco, CA 94158-9001, USA
[3]Departments of Biochemistry and Biophysics, and Cellular and Molecular Pharmacology, University of California, San Francisco, CA 94158-9001, USA
[4]California Institute for Quantitative Biomedical Research, University of California, San Francisco, CA 94158-9001, USA
[5]Kavli Institute for Fundamental Neuroscience, University of California, San Francisco, CA 94158-9001, USA
[6]Molecular Biophysics and Integrated Bio-imaging Division, Lawrence Berkeley National Laboratory, Berkeley, CA 94720, USA
[7]These authors contributed equally
[8]Present address: Department of Genetics, Stanford University, 3165 Porter Drive, Palo Alto, CA 94304, USA
[9]Lead contact
*Correspondence: jdubois@stanford.edu (J.D.), daniel.minor@ucsf.edu (D.L.M.)
https://doi.org/10.1016/j.chembiol.2021.12.003

SUMMARY

Voltage-gated sodium channels (Na_Vs) are targets for a number of acute poisons. Many of these agents act as allosteric modulators of channel activity and serve as powerful chemical tools for understanding channel function. Herein, we detail studies with batrachotoxin (BTX), a potent steroidal amine, and three ester derivatives prepared through *de novo* synthesis against recombinant Na_V subtypes ($rNa_V1.4$ and $hNa_V1.5$). Two of these compounds, BTX-B and BTX-^{c}Hx, are functionally equivalent to BTX, hyperpolarizing channel activation and blocking both fast and slow inactivation. BTX-yne—a C20-*n*-heptynoate ester—is a conspicuous outlier, eliminating fast but not slow inactivation. This property differentiates BTX-yne among other Na_V modulators as a unique reagent that separates inactivation processes. These findings are supported by functional studies with bacterial Na_Vs (BacNa_Vs) that lack a fast inactivation gate. The availability of BTX-yne should advance future efforts aimed at understanding Na_V gating mechanisms and designing allosteric regulators of Na_V activity.

INTRODUCTION

Voltage-gated sodium channels (Na_Vs) are central to physiological function as requisite protein complexes that drive the initiation and propagation of action potentials in electrically excitable cells (Hille, 2001; Peters and Ruben, 2014; Chahine, 2018). Na_V malfunction underlies a number of human pathologies, and, unsurprisingly, acute disruption of Na_V activity can be fatal (Ashcroft, 1999; George, 2005; Fiske, 2006; Catterall, 2008; Lampert, 2010). A large and structurally disparate collection of poisons occur in nature that target Na_Vs (Stevens et al., 2011; Kalia, 2015; Ahern, 2016; Deuis, 2017; Lukowski and Narayan, 2019). The lethality of these agents notwithstanding, peptide and small molecule toxins have proven invaluable as chemical reagents for studies of Na_V structure and dynamics. Among such molecules, one natural product—batrachotoxin (BTX)—is conspicuous. BTX is a steroidal amine derivative commonly associated with poison dart frogs, but also found in species of bird and beetle (Khodorov, 1985; Brown, 1988; Dumbacher et al., 2000, 2004). This toxin is unique among all other Na_V modulators in that it affects every measurable aspect of Na_V function including activation threshold, inactivation, single-channel conductance, and ion selectivity (Catterall et al., 1981; Brown, 1988; Linford et al., 1998; Bosmans, 2004). Because of its chemical complexity and lack of availability from natural sources, studies to dissect how the different structural elements of BTX contribute to altering channel function are limited (Brown et al., 1981; Khodorov et al., 1992; Garraffo and Spande, 2009; Yelin et al., 2019). *De novo* synthesis, however, has enabled access to (−)-BTX and modified forms thereof (Logan, 2016). In this report, experiments comparing the effects of BTX and three BTX C20-ester derivatives against skeletal muscle and cardiac Na_Vs reveal a singular agent, BTX-yne, that differentially influences fast and slow channel inactivation. This unique property distinguishes BTX-yne as a powerful tool for biophysical and pharmacological studies of Na_Vs. The availability of BTX-yne should advance efforts to understand the mechanisms

Please cite this article in press as: MacKenzie et al., Differential effects of modified batrachotoxins on voltage-gated sodium channel fast and slow inactivation, Cell Chemical Biology (2021), https://doi.org/10.1016/j.chembiol.2021.12.003

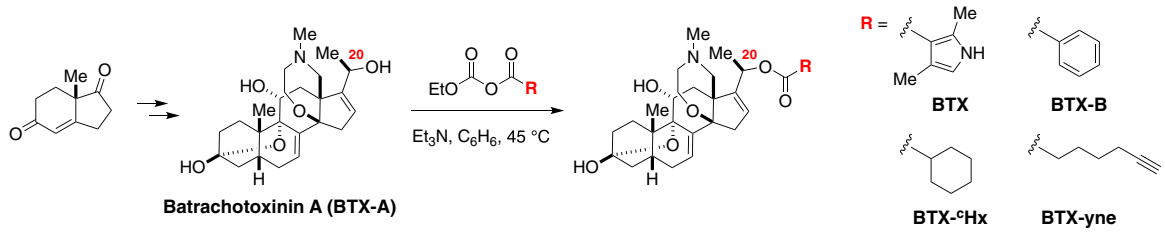

Scheme 1. Synthetic route to BTX C20-ester derivatives

BTX-B = BTX A 20-(*R*)-benzoate; BTX-^{c}Hx = BTX A 20-(*R*)-cyclohexanecarboxylate ester; BTX-yne = BTX A 20-(*R*)-hept-6-ynoate.

underlying Na_V gating and guide the development of allosteric modulators for treating Na_V-related disorders.

Background

Eukaryotic Na_Vs are heteromeric protein complexes consisting of a pore forming α-subunit and up to two auxiliary β-proteins (Catterall, 2012; Ahern, 2016; Chahine, 2018). The α-subunit, of which there are nine different isoforms (Na_V1.1–1.9), derives from a single polypeptide chain that clusters into four homologous repeats (DI–DIV), each consisting of six transmembrane α-helices (S1–S6). Functionally, Na_Vs have two "gates" (activation and inactivation gates), both of which must be open in order for ion conduction to occur (Bezanilla, 2008; Catterall et al., 2017).

The simplest model to describe Na_V gating posits three limiting conformations: 1) a non-conducting closed state that is primed to respond to membrane depolarization; 2) an open, conducting state; and 3) a non-conducting inactivated state (Patlak, 1991). Inactivated channels must transition back to a closed form before firing again. A sufficiently strong membrane depolarization induces the outward movement of the voltage-sensors, causing channels to open (activation). Opening is rapidly followed by inactivation, which occurs on the millisecond timescale (fast inactivation). Fast inactivation involves the movement of a hydrophobic IFM motif located on a loop connecting DIII–DIV, which allosterically effects pore closure (West, 1992; Pan, 2018). An alternative form of Na_V inactivation (slow inactivation) takes place over longer time scales (seconds to minutes) and results from repetitive or sustained membrane depolarization (Vilin et al., 2001; Silva, 2014). Additionally, channels can directly inactivate from the closed state without ever entering the open state (closed-state inactivation) (Goldman, 1995; Armstrong, 2006). The steady-state distribution of closed, open, and inactivated channels at a resting membrane potential is intrinsic to each Na_V α-subunit. Natural toxins and other small molecules that bind the α-subunit are generally biased toward a particular conformational state of the channel and can affect one or more properties such as ion conduction, channel activation, inactivation, and ion selectivity (Wang and Wang, 2003; Stevens et al., 2011; Kalia, 2015; Ahern, 2016; Deuis, 2017; Lukowski and Narayan, 2019). Studies with such agents have been instrumental in dissecting the complex dynamics of channel gating.

Among the most venerable Na_V toxins is the steroidal derivative, BTX, the active component in poison darts obtained from frog secretions by Colombian natives (Märki and Witkop, 1963; Daly, 1965; Tokuyama, 1968, Tokuyama et al., 1969). BTX is the prototypical member of the family of lipid soluble toxins that lodge in the inner pore of the channel (termed site II). These toxins are unique in simultaneously binding to the inner pore and disrupting channel gating. Notably, BTX binding affects every measurable aspect of Na_V function: the activation threshold is shifted in the hyperpolarizing direction by 30–50 mV, both fast and slow inactivation are abolished, single-channel conductance is reduced, and ion selectivity is compromised (Linford et al., 1998; Bosmans, 2004; Wang et al., 2006). Efforts to understand BTX activity have relied on electrophysiology in combination with protein mutagenesis and structure-activity relationship (SAR) studies (Linford et al., 1998; Wang and Wang, 1998, 1999, 2017; Wang et al., 2000, Wang et al., 2001, Wang, 2007; Li et al., 2002; Du et al., 2011). Ligand docking studies with homology models of the Na_V pore suggest specific contacts between toxin and channel but, to date, reveal little about toxin function. The studies detailed herein are enabled by our ability to access BTX through a multistep synthesis (Logan, 2016). This work has led to the identification of BTX-yne, a BTX derivative that alters Na_V gating by inhibiting fast, but not slow, inactivation. This characteristic is distinct from BTX and two other C20-ester variants, all three of which block both fast and slow inactivation. To our knowledge, no other small molecule or peptide has been described that separates these two functional features of the channel.

RESULTS

Synthesis of BTX derivatives

Following our reported synthesis of batrachotoxinin A (BTX-A), we have optimized conditions for modifying the C20 alcohol in order to install different ester groups (Scheme 1). The ester moiety is essential for toxin activity, as BTX-A is > 1,000 times less potent than the parent compound (Albuquerque et al., 1971; Brown, 1988). For the purpose of this study, four compounds were prepared, BTX, BTX-B, BTX-^{c}Hx, and BTX-yne, and evaluated against recombinant rat skeletal muscle sodium channels (rNa_V1.4). The benzoate ester, BTX-B, has been reported previously and is generally regarded as a functional equivalent of BTX (Brown et al., 1981; Catterall et al., 1981); however, a direct quantitative comparison of BTX and BTX-B compounds has not been detailed. The other two derivatives, BTX-^{c}Hx and BTX-yne, were designed to assess the importance of the aryl moiety for toxin activity against Na_V (Tikhonov and Zhorov, 2005; Du et al., 2011). We note that BTX-yne and BTX-^{c}Hx were selected over other ester groups, as these two derivatives are comparable to BTX and BTX-B in terms of lipophilicity based on similar cLogP values (BTX 3.22; BTX-B 4.12; BTX-yne 3.58;

Please cite this article in press as: MacKenzie et al., Differential effects of modified batrachotoxins on voltage-gated sodium channel fast and slow inactivation, Cell Chemical Biology (2021), https://doi.org/10.1016/j.chembiol.2021.12.003

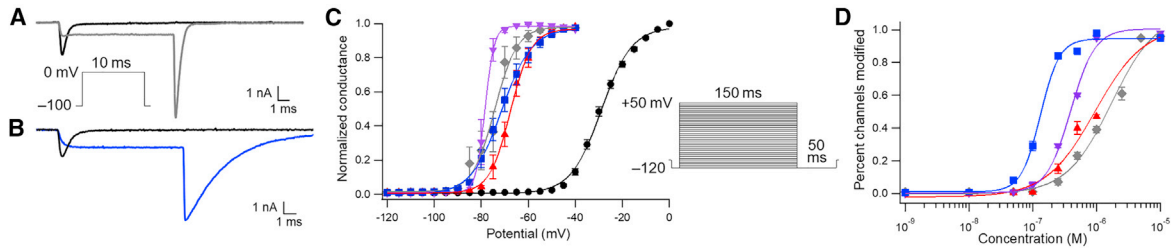

Figure 1. Functional characterization of BTX and BTX derivatives on activation of rNa$_V$1.4

(A) Representative trace for Na$_V$1.4 current before (black) and after (gray) steady-state binding of 10 μM BTX. Current was evoked by a 10-ms test pulse from −100 to 0 mV after establishment of steady-state activity by repetitive depolarizing pulses to 0 mV. Inset: step-depolarization to elicit current response.

(B) Representative trace for Na$_V$1.4 current before (black) and after (blue) steady-state binding of 5 μM BTX-yne. Current was evoked by a 10-ms test pulse from −100 to 0 mV after establishment of steady-state activity by repetitive depolarizing pulses to 0 mV.

(C) Voltage dependence of activation before (black circles) and after application of 10 μM toxin to CHO cells expressing Na$_V$1.4. Inset: stimulation protocol for measuring voltage dependence of channel activation. Normalized conductance was plotted against the recording potential and fit with a sigmoid function; data represent n ≥ 3 ± SEM. Black circles = no compound, gray diamonds = BTX, red triangles = BTX-B, purple inverted triangles = BTX-^{c}Hx, blue squares = BTX-yne.

(D) Concentration-response curve for activation of Na$_V$1.4 by BTX and derivatives (n ≥ 3 ± SEM).

● = untreated rNa$_V$1.4; ◆ = BTX; ▲ = BTX-B; ▼ = BTX-^{c}Hx; ■ = BTX-yne.

BTX-^{c}Hx 4.47). cLogP values were calculated online using MolInspiration (www.molinspiration.com, 2018).

Functional characterization of BTX and BTX derivatives on Na$_V$ activity

Whole-cell voltage-clamp electrophysiology recordings were performed to assay the effects of BTX, along with the other three ester derivatives, against rNa$_V$1.4 transiently expressed in Chinese hamster ovary (CHO) cells. For initial characterization studies, we evaluated all four compounds using the same voltage stimulation protocol. Because BTX is known to preferentially interact with the open state of Na$_V$s, cells treated with toxin were stimulated with 2,000 step pulses from −100 to 0 mV at 2 Hz frequency to promote toxin access to the receptor site (Tanguy and Yeh, 1991). Na$_V$ response to a step depolarization to 0 mV in the absence and presence of BTX is shown in Figure 1A. In contrast to unmodified channels, which quickly reach a peak current and then completely inactivate within 2–3 milliseconds, toxin-modified channels remain open throughout the duration of the step pulse. A large tail current is observed upon hyperpolarization to −100 mV (Figures 1A and D1E). Channels treated with BTX-B and BTX-^{c}Hx present similar current traces (Figures D1I and D1M). By contrast, BTX-yne-modified channels show a marked reduction in the rate of deactivation (Figures 1B and D1Q), suggesting that BTX-yne is more effective than the other three compounds at stabilizing the open state.

Application of BTX to Na$_V$1.4 has a pronounced influence on the threshold potential at which channels open, shifting the half-activation potential ($V_{½\ act}$) by −45 mV. Using the same multistep activation protocol, we measured the influence of BTX derivatives (10 μM) on this value (Figures 1C and S1). The resulting activation curves show that all three derivatives have effects similar to BTX on threshold activation, albeit with small differences in the slope factors (k) (Figures 1C, Table 1). Activation curves obtained at a sub-saturating concentration of toxin were fitted by a sum of two Boltzmann equations, revealing two populations of channels: 1) toxin-modified channels with more negative $V_{1/2\ act}$ values and 2) unmodified channels with typical Na$_V$1.4 $V_{½\ act}$ values of −30 mV (Figure S1, Table S1). At 100 nM toxin, the extent to which channel activation is altered differs between the four compounds (Figure S1; Table S1). To determine EC$_{50}$ values, the effect of toxins at different concentrations on channel activation was measured (Figures 1D and S1, D1). Based on this analysis, BTX-yne is the most potent compound with an EC$_{50}$ that is ∼16 times lower than BTX itself.

The relative potencies of BTX and BTX derivatives against Na$_V$1.4 can be further assessed by considering either the ratio of sustained current/peak current or the ratio of tail current/peak current resulting from a strong depolarization (Li et al., 2002; Wang and Wang, 2017). We evaluated the four toxins in both ways and found toxin activities to mirror EC$_{50}$ data (Figure 2D S2, and D2, Table S2). Our findings validate and demonstrate the equivalency of such protocols for quantitatively analyzing the action of these compounds.

BTX derivatives differentially influence Na$_V$ inactivation

A signature effect of BTX on Na$_V$ activity is the elimination of both fast and slow inactivation (Figure 1A). To determine if C20-ester substitution of the toxin alters this behavior, we used a two-pulse protocol to measure steady-state inactivation (SSI) (Figure 2 inset) Bendahhou et al., 1999). Channels that inactivate in the pre-pulse period are unavailable to open in the test pulse. A plot of normalized current versus voltage (I/I_o–V) for unmodified channels (black circles) under this SSI protocol is shown in Figure 2C. Analogous SSI curves for toxin-treated Na$_V$s display similar Boltzmann behavior, but a fraction of the total population of channels is non-inactivating; this percentage varies in a dose-dependent manner (Figures S3 and D2, Table S3). At saturating concentrations of BTX, BTX-B, and BTX-^{c}Hx, inactivation is completely abrogated (Figures 2A, S3, D2). EC$_{50}$ values for the SSI response were determined by varying toxin concentration (Table 1). These values accord with voltage of activation EC$_{50}$s for each compound.

Comparison of SSI curves recorded at saturating concentration (10 μM) of each of the four toxin derivatives reveals an unexpected difference for BTX-yne (Figures 2A–2C, S3). In contrast to BTX, BTX-B, and BTX-^{c}Hx, which eliminate inactivation, BTX-yne-modified channels are able to inactivate partially. Interestingly, a plot of I/I_0 versus voltage appears as a U-shaped SSI curve (*vide infra*). The extent to which BTX-yne-treated channels

Please cite this article in press as: MacKenzie et al., Differential effects of modified batrachotoxins on voltage-gated sodium channel fast and slow inactivation, Cell Chemical Biology (2021), https://doi.org/10.1016/j.chembiol.2021.12.003

Table 1. Boltzmann fit and affinity parameters for untreated and toxin-modified rNa$_V$1.4

Toxin	$V_{1/2\ act}$ (mV)	$\Delta V_{1/2\ act}$ (mV)	k (mv)	EC_{50} (nM)	EC_{50} (from SSI)
None	−28.9 ± 0.3	–	6.5 ± 0.3	–	–
BTX	−74.3 ± 0.6	−45.4 ± 0.7	4.8 ± 0.5	2074 ± 768	2237 ± 1120
BTX-B	−67.5 ± 0.2	−38.6 ± 0.4	4.5 ± 0.2	756 ± 43	795 ± 113
BTX-^{c}Hx	−78.4 ± 0.1	−49.5 ± 0.3	2.0 ± 0.1	491 ± 26	494 ± 37
BTX-yne	−71.4 ± 0.3	−42.7 ± 0.4	6.5 ± 0.3	130 ± 21	189 ± 59

are inactivated can be estimated by applying a baseline correction to the SSI curve (Figure S4). From this analysis, 40%–50% of channel inactivation occurs at a saturating concentration of BTX-yne, as compared with ca. 100% and 0% for untreated and BTX-B-modified channels, respectively. The influence of BTX-yne on SSI is not unique to rNa$_V$1.4, as hNa$_V$1.5 channels treated with this compound (5 μM) are similarly altered (Figure S5).

Although all four toxin derivatives shift the activation voltage dependence to a comparable extent, BTX-yne stands alone as the only compound that does not completely inhibit channel inactivation (Figures 1C and 2C). Superposition of the voltage-dependent activation and inactivation curves shows that, in the presence of BTX-yne, inactivation initiates at potentials at which channels are closed (<−100 mV) and persists even when all channels are open (>−40 mV) (Figures S4E–S4F). This observation suggests that BTX-yne-modified channels undergo inactivation from both the closed and open states (i.e., closed-state and open-state inactivation, respectively). Recording data shown in Figure 1B illustrate that BTX-yne blocks Na$_V$1.4 fast inactivation, analogous to the other three agents (Figures S3 and D2). The question thus arises: can BTX-yne-modified channels transition to a non-conducting state through slow inactivation? To address this question, we first determined the time constant for BTX-yne-modified channels to undergo slow inactivation at −70 mV. This potential was chosen as it represents the lowest point of the U-shaped SSI curve (i.e., the point at which maximum inactivation is evident in the raw current recording).

Cells were stepped from a holding potential of −120 to −70 mV for varying lengths of time, Δt. Following this conditioning pulse, the extent to which channels inactivate as a function of Δt was measured in a test pulse to 0 mV (Figure S6) (Cummins et al., 1998). BTX-B was employed as a negative control for these experiments, as channels bound to this compound remain conducting irrespective of the time period of the conditioning or test pulses. Using this stimulation protocol, cells treated with 10 μM BTX-yne display a clear exponential decay of peak current as a function of the conditioning pulse length. Fitting these data for BTX-yne to two exponentials gives a time constant, τ, for each process (τ_{fast} = 90.8 ± 3.8 ms; τ_{slow} = 929.9 ± 325.1 ms). Accordingly, a stimulation protocol to measure slow inactivation of BTX-yne-modified channels requires conditioning pulses >> 1,000 ms in duration to ensure that equilibrium is achieved between successive current recordings.

The effect of each toxin on slow inactivation was examined using the stimulation protocol shown in Figure 3A (inset). A conditioning pulse was applied from −140 to 0 mV in 5 mV increments over a 6,500-ms interval (6.5 x τ_{slow}). Following the pre-pulse, a 150-ms test pulse to 0 mV measured channel availability. In unmodified channels, a brief hyperpolarizing step (10 ms) to −120 mV was included to recover from fast inactivation (not shown in Figure 3A, see Figure S7). The addition of this step pulse is both unnecessary and problematic in recordings of toxin-modified channels—the former because all four compounds block fast inactivation, the latter stemming from the large and variable tail currents, which interfere with measurements in the test pulse.

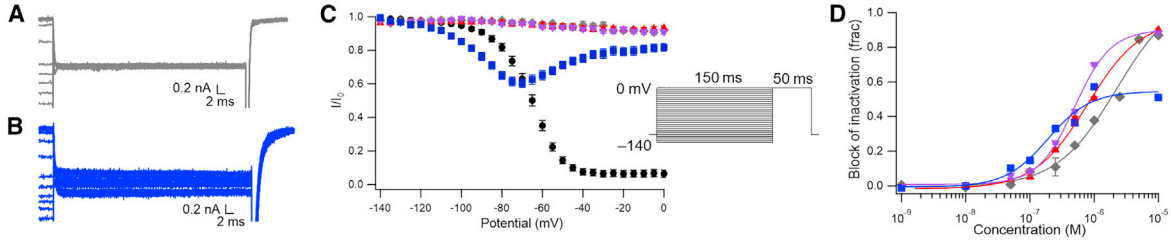

Figure 2. Steady-state inactivation of rNa$_V$1.4 modified by BTX and BTX derivatives

(A) Representative trace for Na$_V$1.4 current after (gray) steady-state binding of 10 μM BTX during the test pulse of the inactivation protocol (C, inset). Current was evoked by a 50-ms test pulse from −100 to 0 mV after establishment of steady-state activity by repetitive depolarizing pulses to 0 mV and following a variable conditioning pulse.

(B) Representative trace for Na$_V$1.4 current after (blue) steady-state binding of 5 μM BTX-yne using the same inactivation protocol as in (A).

(C) Voltage dependence of inactivation before (black circles) and after application of 10 μM of the indicated toxin to CHO cells expressing Na$_V$1.4. Data were recorded using the stimulation protocol shown in the inset. Normalized current (I/I_0) in the test pulse was plotted against the conditioning potential; data represent n ≥ 3 ± SEM. Black circles = no compound, gray diamonds = BTX, red triangles = BTX-B, purple inverted triangles = BTX-^{c}Hx, blue squares = BTX-yne. (D) Concentration-response curve for block of inactivation of Na$_V$1.4 by BTX and derivatives (n ≥ 3 ± SEM).

● = untreated rNa$_V$1.4; ◆ = BTX; ▲ = BTX-B; ▼ = BTX-^{c}Hx; ■ = BTX-yne.

Please cite this article in press as: MacKenzie et al., Differential effects of modified batrachotoxins on voltage-gated sodium channel fast and slow inactivation, Cell Chemical Biology (2021), https://doi.org/10.1016/j.chembiol.2021.12.003

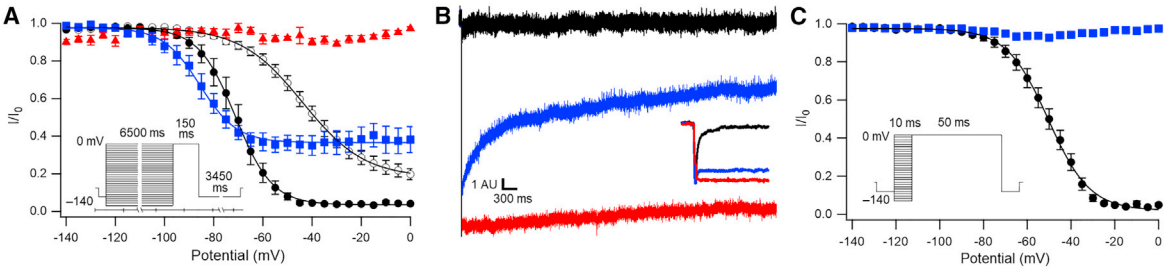

Figure 3. Characterization of slow inactivation for rNa$_V$1.4 modified by BTX-B and BTX-yne

(A) Voltage dependence of slow inactivation before (black circles) and after application of 10 μM BTX-B (red triangles) or BTX-yne (blue squares). Inset: stimulation protocol for measuring voltage dependence of slow inactivation (note the truncated x axis). Normalized current in the test pulse was plotted against the conditioning potential and fit with a sigmoid function; data represent n ≥ 3 ± SEM. Open circles represent unmodified channels recorded with a hyperpolarizing step after the conditioning pulse to account for fast-inactivated channels; see Figure S7 for details.

(B) Representative trace for Na$_V$1.4 current before (black) and following application of 10 μM BTX-B (red) or BTX-yne (blue). Current was evoked by a 6,500-ms test pulse from −100 to 0 mV after steady state was obtained through repetitive depolarizing pulses to 0 mV. Note that the y axis units are arbitrary as the peak current for each trace has been normalized to the same magnitude. Inset shows the first 20 ms of the same trace.

(C) Voltage dependence of fast inactivation before (black circles) and following application of 10 μM BTX-yne (blue squares). Inset: stimulation protocol for measuring voltage dependence of fast inactivation. Normalized current in the test pulse was plotted against the conditioning potential and fit with a sigmoid function; data represent n ≥ 3 ± SEM.

Using the protocol shown in Figure 3A (inset), absent a hyperpolarizing step to recover from fast inactivation, the inactivation response of unmodified channels (black circles) displays sigmoidal behavior (Figure 3A). When a 10-ms hyperpolarizing step to −120 mV is included to enable channels to recover from fast inactivation, the voltage dependence of SSI is shallower (i.e., larger k value) and shifted considerably to higher potential, and normalized current (I/I_0) never reaches zero (open circles). Channels modified by 10 μM BTX-B do not inactivate in either the conditioning or the test pulse (Figures 3A and 3B, red triangles), analogous to BTX (Wang and Wang, 1994, 1996). By contrast, channels modified with 10 μM BTX-yne exhibit a clear voltage-dependent slow inactivation with current decaying to a steady-state value that is ~60% of the peak current, I_0 (Figures 3A and 3B, blue squares). Two principal conclusions follow from these data: 1) ~80% of unmodified channels enter a slow-inactivated state (open circles, Figure 3C); 2) BTX-yne-modified channels are able to undergo slow inactivation. The latter finding is in marked contrast to channels treated with BTX-B, for which both fast and slow inactivation are entirely inhibited.

To obtain additional support for the above conclusions, we used an amended stimulation protocol to measure fast inactivation (Figure 3C, inset). In these experiments, a short conditioning pulse (10 ms) only allows time for channels to undergo fast inactivation. Accordingly, application of 10 μM BTX-yne to cells under this protocol gives no evidence of inactivation (Figure 3C). In fact, these data look indistinguishable from the inactivation plots of other BTX derivatives (Figure 2B). These results confirm that BTX-yne prevents fast inactivation and that BTX-yne-modified channels are able to access the slow-inactivated state.

BTX derivatives differentially affect bacterial Na$_V$ inactivation

Our findings with Na$_V$1.4 and Na$_V$1.5 implicate BTX-yne as an inhibitor of fast but not slow inactivation. To interrogate further the activity of this toxin derivative, we have examined the influence of BTX-yne as well as BTX, BTX-B, and BTX-^{c}Hx on Na$_V$s that lack a fast inactivation gate. Bacterial Na$_V$s (BacNa$_V$s) form as homotetramers of non-covalently associated domains, analogous to voltage-gated K^+ channels, and lack the DIII–DIV linker and IFM particle (or a functional equivalent) responsible for fast inactivation in eukaryotic channels (Payandeh and Minor Jr., 2015; Lenaeus et al., 2017; Payandeh, 2018). Thus, only one form of inactivation is operative in BacNa$_V$s.

We initially examined Na$_V$Bh1 (NachBac), a well-studied BacNa$_V$ that is sensitive to BTX (Finol-Urdaneta et al., 2019). In line with our work and previous reports of BTX activity against eukaryotic Na$_V$s, toxin application (10 μM) stabilized the Na$_V$Bh1 open state and shifted the activation voltage dependence toward hyperpolarizing potentials (Figures S8A, S8B, and S8D). Unlike eukaryotic Na$_V$s, however, Na$_V$Bh1 proved surprisingly insensitive to BTX-B (Figures S8C and S8D). An alternative BacNa$_V$, Na$_V$Ae1, from *Alkalilimnicola ehrlichii* (Arrigoni et al., 2016) bearing a mutation in the cytosolic C-terminal domain "neck region" (R264E) to enable functional studies (Shaya et al., 2014) was only modestly influenced by BTX (Figures S8E–S8G). To understand these unexpected differences in toxin activity, we examined sequence alignments of the inner pore S6 helices of select bacterial and eukaryotic channels (Figure S8H). This analysis identified a serine residue in the Na$_V$Ae1 inner pore that appears as a glycine in Na$_V$Bh1 and in three of the four S6 helices in eukaryotic Na$_V$s (Figures S8H–S8I). Mutation of S225 to glycine (S225G) in Na$_V$Ae1 R264E yields a channel that is sensitive to both BTX and BTX-B (Figures 4A–4C and S8J–S8K) as well as BTX-^{c}Hx and BTX-yne (Figures 4D and 4E). All four compounds cause substantial hyperpolarizing shifts in activation and inhibit channel inactivation (Figures 4A–4F). Electrophysiology recordings to measure steady-state inactivation confirm that BTX, BTX-B, and BTX-^{c}Hx significantly block inactivation of Na$_V$Ae1 S225G-R264E (Figures 4B–4D and 4G). In marked contrast, Na$_V$Ae1 S225G-R264E channels exposed to BTX-yne show a strong SSI response, as noted in unmodified channels (Figure 4G). This result offers compelling evidence that BTX-yne, unlike the other three compounds, is ineffective at blocking inactivation in this mutant BacNa$_V$.

Please cite this article in press as: MacKenzie et al., Differential effects of modified batrachotoxins on voltage-gated sodium channel fast and slow inactivation, Cell Chemical Biology (2021), https://doi.org/10.1016/j.chembiol.2021.12.003

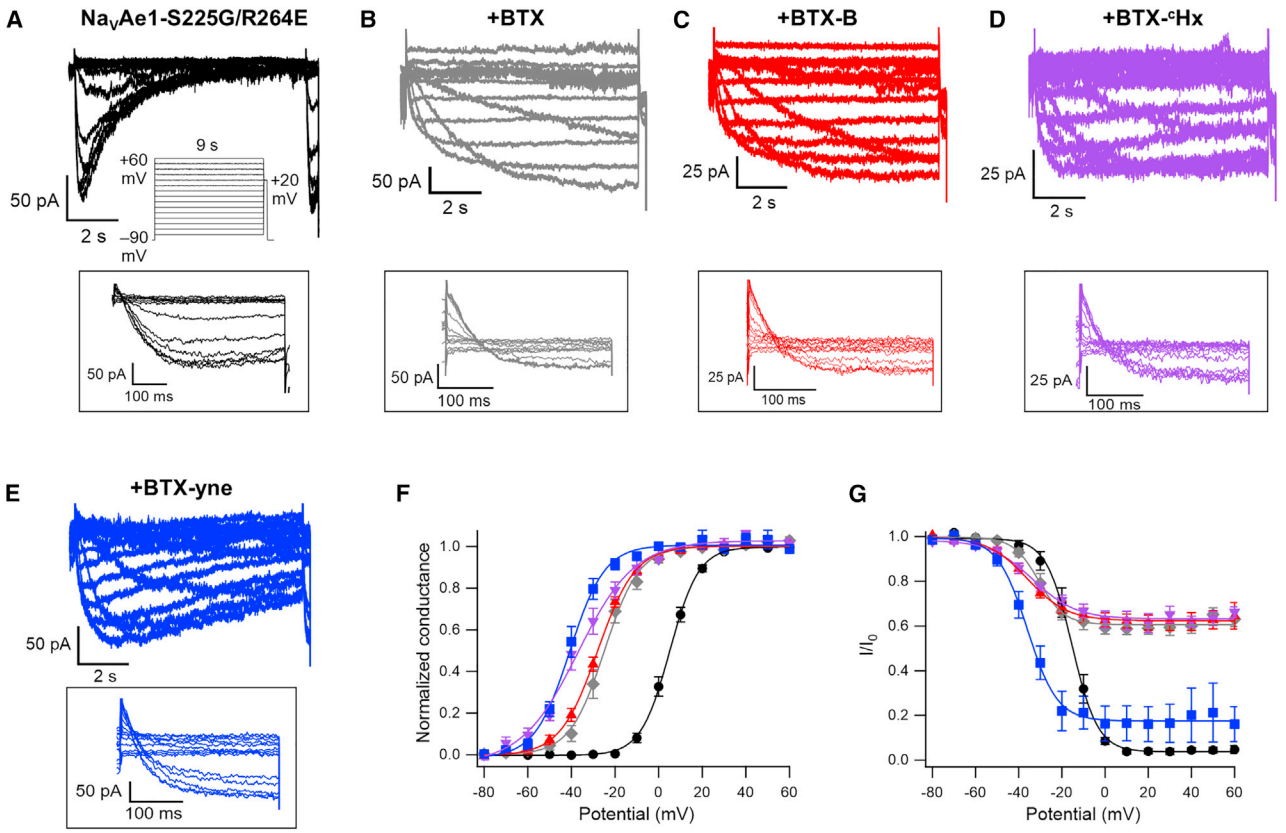

Figure 4. Functional characterization of BTX and BTX derivatives on BacNa$_V$ activity

(A–E) Representative current recordings for Na$_V$Ae1-S225G/R264E before (A) and after application of 10 μM BTX (B), BTX-B (C), BTX-^{c}Hx (D), and BTX-yne (E) in response to an inactivation protocol. Traces shown in insets are magnifications of the current in response to the +20-mV test pulse.

(F and G) (F) Activation and (G) inactivation voltage dependence for Na$_V$Ae-S225G/R264E before (black circle) and after application of 10 μM BTX (gray diamonds), BTX-B (red triangles), BTX-^{c}Hx (purple inverted triangles), or BTX-yne (blue squares). Data represent n ≥ 6 ± SEM.

● = untreated rNa$_V$1.4; ◆ = BTX; ▲ = BTX-B; ▼ = BTX-^{c}Hx; ■ = BTX-yne.

DISCUSSION

We have synthesized BTX and three C20-ester derivatives and characterized these compounds by whole-cell electrophysiology against rNa$_V$1.4. All four compounds significantly hyperpolarize $V_{1/2}$ of activation, albeit with some variation in the magnitude of this effect (see Table 1). We have examined different protocols to measure the influence of non-saturating toxin concentrations on channel activity and have established that these methods give similar outputs (Li et al., 2002; Wang and Wang, 2017). Concentration-response measurements quantify the relative activity of BTX, BTX-B, BTX-^{c}Hx, and BTX-yne. The potencies of BTX, BTX-B, and BTX-^{c}Hx, the three derivatives that eliminate fast and slow inactivation, track with cLogP values for these compounds (cLogP: 3.22, 4.12, 4.47; EC_{50} for $V_{1/2}$ activation: 2074 nM, 756 nM, 491 nM, respectively).[23] This trend is consistent with toxin binding at site II, as the inner pore of the channel is a receptor for hydrophobic molecules. To our knowledge, this work represents the first systematic analysis of toxin potency against a recombinant Na$_V$ subtype.

The influence of BTX on channel inactivation is pronounced, as channels remain persistently conducting, unable to conformationally rearrange in a manner that stops the flow of ions (Khodorov, 1985; Brown, 1988). Our findings demonstrate that BTX-B and BTX-^{c}Hx, like the parent toxin, block fast and slow inactivation mechanisms. Channels modified by BTX-yne are also prevented from rapidly inactivating. BTX-yne binding, however, does not preclude channels from undergoing a slow, voltage-dependent transition to a non-conducting state. Slow inactivation is thought to involve extensive protein conformational changes, but a structural understanding of this process is still lacking (Cummins and Sigworth, 1996; Featherstone et al., 1996; Hayward et al., 1997; Vedantham and Cannon, 1998; Vilin et al., 2001; Hilber et al., 2002; Wang et al., 2003; Webb et al., 2009). Toxin derivatives such as BTX-yne should aid studies of this intriguing gating mechanism.

Additional evidence that BTX-yne is unable to block slow inactivation follows from investigations with the bacterial sodium channel mutant, Na$_V$Ae1 S225G-R264E. As with other BacNa$_V$s, Na$_V$Ae1 S225G-R264E lacks a fast inactivation particle and, thus, has only one mechanism for transitioning from an open to a non-conducting state. Electrophysiological recordings of Na$_V$Ae1 S225G-R264E following treatment with BTX, BTX-B, or BTX-^{c}Hx display essentially equivalent effects in which all three compounds induce a large hyperpolarizing shift in activation voltage dependence and block inactivation (Figures 4B–4D, 4F, and 4G). These

Please cite this article in press as: MacKenzie et al., Differential effects of modified batrachotoxins on voltage-gated sodium channel fast and slow inactivation, Cell Chemical Biology (2021), https://doi.org/10.1016/j.chembiol.2021.12.003

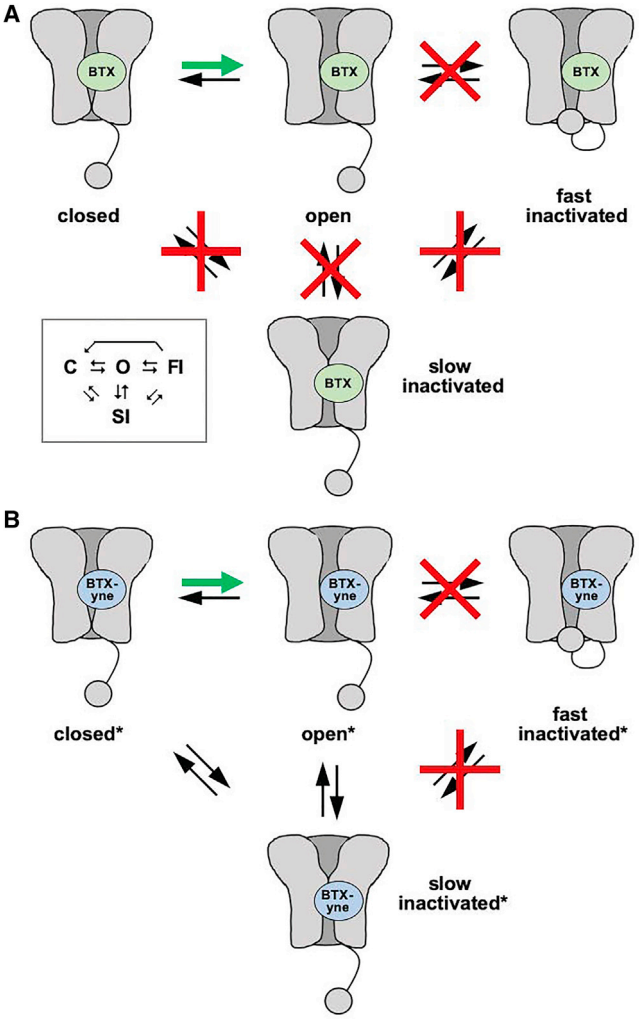

Figure 5. A simplified schematic diagram detailing the influence of toxin binding on the transitions between limiting Na_V conformational states

(A) Inset: four-state gating model for unmodified Na_V (C = closed, O = open, FI = fast inactivated; SI = slow inactivated); BTX (and BTX-B, BTX-^{c}Hx) facilitates the C→O transition (green arrow) and blocks both fast and slow inactivation.

(B) BTX-yne facilitates the C→O transition (green arrow) and blocks fast inactivation; modified channels can transition from closed* and open* to a slow-inactivated* state. Data represent n ≥ 6 ± SEM.

data are similar to results with eukaryotic channels, $Na_V1.4$ and 1.5. By contrast, Na_VAe1 S225G-R264E channels modified by BTX-yne, for which activation voltage is significantly hyperpolarized, can enter a non-conducting state (Figures 4E–4G) The inability of BTX-yne to block inactivation in Na_VAe1 S225G-R264E supports our conclusion that this same compound is incapable of blocking slow inactivation in mammalian Na_Vs.

A simplified four-state model is sufficient to appreciate the differences between BTX and BTX-yne on Na_V gating (for a recent, comprehensive discussion on Na_V gating, see Catterall et al., 2020). Closed channels, unmodified by toxin, can enter either an open (conductive) or slow-inactivated (non-conductive) state (Figure 5A). The degree to which either pathway is favored is voltage-dependent. Open channels quickly become non-conducting through a mechanism of fast inactivation and a secondary inactivation pathway that is kinetically slower. BTX, as well as BTX-B and BTX-^{c}Hx, facilitates the closed→open transition and blocks both inactivation processes; thus, channels open upon membrane depolarization at more negative potentials and remain conductive.

As with BTX, BTX-yne influences the steady-state population of closed*⇆open* channels and inhibits fast inactivation (note: * reflects BTX-yne-bound channels, Figure 5B). Channel inactivation, however, through closed*⇆slow-inactivated* (i.e., closed-state inactivation) and open*⇆slow-inactivated* transitions, is not blocked by BTX-yne. The combination of 1) inhibition of fast inactivation and 2) slow conversion from the open*→slow-inactivated* state relative to the time duration of the conditioning pulse (150 ms) in the SSI protocol gives rise to the unusual U-shaped SSI curve for BTX-yne-modified Na_Vs (see Figure 2B). As conditioning pulses in the SSI protocol are stepped to higher depolarizing potentials, the fraction of channels transitioning from closed*→slow inactivated* first increases in a voltage-dependent manner, leading to the downstroke of the current versus voltage response, which reaches a nadir at −70 mV. Conditioning depolarizations > −70 mV result in fewer channels undergoing closed-state inactivation, leaving a larger number of channels available to activate. Open* channels cannot fast inactivate and do not have sufficient time to slow inactivate* given the 150-ms duration of the conditioning pulse (recall that τ_{slow} = 930 ms, Figure S6). As such, an increase in current is measured at higher step potentials (the upstroke of the U-shaped curve). This interpretation is consistent with the absence of a U-shaped SSI curve for BTX-yne-modified Na_Vs with longer (6,500 ms) conditioning pulses (Figure 3A).

For a derivative of BTX to function equivalently to the natural product, the full pentacyclic steroidal core as well as an ester substituent at C20 are necessary. Studies with semi-synthetic BTX derivatives demonstrate that removal of the C20-ester results in compounds that lose considerable potency (Figure S9) (Khodorov et al., 1992). Reduction in the B-ring double bond in BTX affords a toxin derivative that hyperpolarizes $V_{1/2}$, but no longer completely blocks inactivation. Synthetic analogues of the AB-ring of BTX containing pendant amine groups antagonize BTX binding, but do not hyperpolarize $V_{1/2}$ or eliminate inactivation (Schow et al., 1997). Additionally, analogues of the CDE-ring of BTX act as reversible Na_V inhibitors despite binding in the inner pore of the channel (Toma et al., 2016). Like these compounds, the enantiomer of BTX also functions as a channel antagonist with a binding site that overlaps that of the natural product (Logan, 2016).

Collectively, our findings reveal that the intrinsic rigidity of BTX, including the heteroaryl C20-ester substituent, is critical to agonist function. Modified forms of the toxin that have additional degrees of flexibility (e.g., reduced B-ring double bond, CDE-ring analogues, C20-hexynoate ester) may adopt binding poses that either block ion conduction or enable the channel to enter a partially inactivated conformational state. BTX-yne is the first small molecule tool compound that selectively eliminates Na_V fast, but not slow, inactivation. Such a reagent should enable research efforts to explore channel dynamics and the mechanism of this latter process.

CONCLUSION

Our studies to examine structure-activity relationships of BTX and a small collection of ester-modified toxins reveal the complex allosteric properties of these ligands on Na_V function. This work provides a complete electrophysiological characterization of toxin affinity and the effects of toxin binding on both channel activation and inactivation. We have identified a BTX ester derivative, BTX-yne, that affects fast and slow inactivation processes in a manner that is differential from BTX and from any other small molecule or protein toxin modulator of Na_Vs. Future studies will aim to shed light on the molecular details of BTX and BTX-yne binding to the channel. Such insights are expected to inform the rational design of small molecule Na_V modulators that offer precise control of gating.

SIGNIFICANCE

Na_Vs are obligatory protein complexes for generating electrical signals in neuronal cells. These molecular machines operate through complex mechanisms in order to regulate the flow of sodium ions across cellular membranes. Understanding how Na_Vs function and how small molecules that target these channels modulate ion conduction will inform efforts in pharmaceutical research to design precision therapeutics for treating Na_V-related pathologies.

STAR★METHODS

Detailed methods are provided in the online version of this paper and include the following:

- KEY RESOURCES TABLE
- RESOURCE AVAILABILITY
  - Lead contact
  - Materials availability
  - Data and code availability
- EXPERIMENTAL MODEL AND SUBJECT DETAILS
  - CHO and HEK cell cultures
- METHOD DETAILS
  - Transient transfection of Na_V plasmids
  - Toxin quantification and storage
  - Electrophysiology
  - Chemistry: general experimental
  - Synthetic experimental procedures
- QUANTIFICATION AND STATISTICAL ANALYSIS

SUPPLEMENTAL INFORMATION

Supplemental information can be found online at https://doi.org/10.1016/j.chembiol.2021.12.003.

ACKNOWLEDGMENTS

Partial support of this work has come from the National Institutes of Health (R01 NS045684) and from a generous gift from Amgen, Inc. T.M.G.M. was supported by a fellowship from the Center for Molecular Analysis and Design (CMAD) at Stanford University. C.E.G. is grateful for support from the Stanford ChEM-H Chemistry/Biology Interface Predoctoral Training Grant Program and the NIGMS of the NIH under Award Number T32GM120007 and to Abbott Laboratories for a Stanford Graduate Fellowship. This work was supported by grants NIH-NHLBI R01-HL080050 and NIH-NIDCD R01-DC007664 to D.L.M. and an American Heart Association postdoctoral fellowship to F.A.-A.

AUTHOR CONTRIBUTIONS

T.M.G.M. and J.D. originally conceived of the project. T.M.G.M., F.A.A., and C.E.G. performed research; all authors were involved in analyzing the data. T.M.G.M. and J.D. wrote the paper with input from C.E.G., F.A.A., and D.L.M.

DECLARATION OF INTERESTS

J.D. is a cofounder, executive board member, and holds equity shares in SiteOne Therapeutics, Inc., a start-up company interested in developing subtype-selective modulators of Na_V.

Received: February 22, 2021
Revised: September 14, 2021
Accepted: November 29, 2021
Published: December 27, 2021

REFERENCES

Ahern, C.A., Payandeh, J., Bosmans, F., and Chanda, B. (2016). The hitchhiker's guide to the voltage-gated sodium channel galaxy. J. Gen. Physiol. *147*, 1–24. https://doi.org/10.1085/jgp.201511492.

Albuquerque, E.X., Daly, J.W., and Witkop, B. (1971). Batrachotoxin: chemistry and pharmacology. Science *172*, 995–1002. https://doi.org/10.1126/science.172.3987.995.

Andresen, B.M., and Du Bois, J. (2009). De novo synthesis of modified saxitoxins for sodium ion channel study. J. Am. Chem. Soc. *131*, 12524–12525. https://doi.org/10.1021/ja904179f.

Armstrong, C.M. (2006). Na channel inactivation from open and closed states. Proc. Natl. Acad. Sci. U S A *103*, 17991–17996. https://doi.org/10.1073/pnas.0607603103.

Arrigoni, C., Rohaim, A., Shaya, D., Findeisen, F., Stein, R.A., Nurva, S.R., Mishra, S., McHaourab, H.S., and Minor, D.L. (2016). Unfolding of a Temperature-Sensitive Domain Controls Voltage-Gated Channel Activation. Cell *164*, 922–936. https://doi.org/10.1016/j.cell.2016.02.001.

Ashcroft, F.M. (1999). Ion channels and disease. Academic Press, Inc.

Bendahhou, S., Cummins, T.R., Tawil, R., Waxman, S.G., and Ptácek, L.J. (1999). Activation and inactivation of the voltage-gated sodium channel: role of segment S5 revealed by a novel hyperkalaemic periodic paralysis mutation. J. Neurosci. *19*, 4762–4771. https://doi.org/10.1523/jneurosci.19-12-04762.1999.

Bezanilla, F. (2008). How membrane proteins sense voltage. Nat. Rev. Mol. Cell Biol. *9*, 323–332. https://doi.org/10.1038/nrm2376.

Bosmans, F., Maertens, C., Verdonck, F., and Tytgat, J. (2004). The poison dart frog's batrachotoxin modulates Na_V1.8. FEBS Lett. *577*, 245–248. https://doi.org/10.1016/j.febslet.2004.10.017.

Brown, G.B., Tieszen, S.C., Daly, J.W., Warnick, J.E., and Albuquerque, E.X. (1981). Batrachotoxinin-A 20-α-benzoate: a new radioactive ligand for voltage sensitive sodium channels. Cell Mol. Neurobiol. *1*, 19–40. https://doi.org/10.1007/BF00736037.

Brown, G.B. (1988). Batrachotoxin: a window on the allosteric nature of the voltage-sensitive sodium channel. Int. Rev. Neurobiol. *29*, 77–116. https://doi.org/10.1016/S0074-7742(08)60084-7.

Catterall, W.A., Morrow, C.S., Daly, J.W., and Brown, G.B. (1981). Binding of batrachotoxinin A 20-α-benzoate to a receptor site associated with sodium channels in synaptic nerve ending particles. J. Biol. Chem. *256*, 8922–8927. https://doi.org/10.1016/s0021-9258(19)52487-5.

Catterall, W.A., et al. (2008). Inherited neuronal ion channelopathies: new windows on complex neurological diseases. J. Neurosci. *28*, 11768–11777. https://doi.org/10.1523/JNEUROSCI.3901-08.2008.

Catterall, W.A. (2012). Voltage-gated sodium channels at 60: structure, function and pathophysiology. J. Physiol. *590*, 2577–2589. https://doi.org/10.1113/jphysiol.2011.224204.

Catterall, W.A., Wisedchaisri, G., and Zheng, N. (2017). The chemical basis for electrical signaling. Nat. Chem. Biol. *13*, 455–463. https://doi.org/10.1038/nchembio.2353.

Catterall, W.A., Wisedchaisri, G., and Zheng, N. (2020). The conformational cycle of a prototypical voltage-gated sodium channel. Nat. Chem. Biol. *16*, 1314–1320. https://doi.org/10.1038/s41589-020-0644-4.

Chahine, M. (2018). In Voltage-gated Sodium Channels: Structure, Function and Channelopathies, Handbook of Experimental Pharmacology, M. Chahine, ed. (Springer International Publishing). https://doi.org/10.1007/978-3-319-90284-5.

Cummins, T.R., Howe, J.R., and Waxman, S.G. (1998). Slow closed-state inactivation: a novel mechanism underlying ramp currents in cells expressing the hNE/PN1 sodium channel. J. Neurosci. *18*, 9607–9619. https://doi.org/10.1523/jneurosci.18-23-09607.1998.

Cummins, T.R., and Sigworth, F.J. (1996). Impaired slow inactivation in mutant sodium channels. Biophysical J. *71*, 227–236. https://doi.org/10.1016/S0006-3495(96)79219-6.

Daly, J.W., Witkop, B., Bommer, P., and Biemann, K. (1965). Batrachotoxin. The active principle of the Colombian arrow poison frog, *Phyllobates bicolor*. J. Am. Chem. Soc. *87*, 124–126. https://doi.org/10.1021/ja01079a026.

Deuis, J.R., Mueller, A., Israel, M.R., and Vetter, I. (2017). The pharmacology of voltage-gated sodium channel activators. Neuropharmacology *127*, 87–108. https://doi.org/10.1016/j.neuropharm.2017.04.014.

Du, Y., Garden, D.P., Wang, L., Zhorov, B.S., and Dong, K. (2011). Identification of new batrachotoxin-sensing residues in segment IIIS6 of the sodium channel. J. Biol. Chem. *286*, 13151–13160. https://doi.org/10.1074/jbc.M110.208496.

Dumbacher, J.P., Spande, T.F., and Daly, J.W. (2004). Melyrid beetles (Choresine): a putative source for the batrachotoxin alkaloids found in poison-dart frogs and toxic passerine birds. Proc. Natl. Acad. Sci. U S A *101*, 15857–15860. https://doi.org/10.1073/pnas.0407197101.

Dumbacher, J.P., Spande, T.F., and Daly, J.W. (2000). Batrachotoxin alkaloids from passerine birds: a second toxic bird genus (Ifrita kowaldi) from New Guinea. Proc. Natl. Acad. Sci. U S A *97*, 12970–12975. https://doi.org/10.1073/pnas.200346897.

Featherstone, D.E., Richmond, J.E., and Ruben, P.C. (1996). Interaction between fast and slow inactivation in Skm1 sodium channels. Biophysical J. *71*, 3098–3109. https://doi.org/10.1016/S0006-3495(96)79504-8.

Finol-Urdaneta, R.K., McArthur, J.R., Goldschen-Ohm, M.P., Gaudet, R., Tikhonov, D.B., Zhorov, B.S., and French, R.J. (2019). Batrachotoxin acts as a stent to hold open homotetrameric prokaryotic voltage-gated sodium channels. J. Gen. Physiol. *151*, 186–199. https://doi.org/10.1085/jgp.201812278.

Fiske, J.L., Fomin, V.P., Brown, M.L., Duncan, R.L., and Sikes, R.A. (2006). Voltage-sensitive ion channels and cancer. Cancer Metastasis Rev. *25*, 493–500. https://doi.org/10.1007/s10555-006-9017-z.

Garraffo, H.M., and Spande, T.F. (2009). Discovery of batrachotoxin: the launch of the frog alkaloid program at NIH. Heterocycles *79*, 195–205. https://doi.org/10.3987/REV-08-SR(D)6.

George, A.L. (2005). Inherited disorders of voltage-gated sodium channels. J. Clin. Invest. *115*, 1990–1999. https://doi.org/10.1172/JCI25505.

Goldman, L. (1995). Sodium channel inactivation from closed states: evidence for an intrinsic voltage dependency. Biophysical J. *69*, 2369–2377. https://doi.org/10.1016/S0006-3495(95)80106-2.

Hayward, L.J., Brown, R.H., and Cannon, S.C. (1997). Slow inactivation differs among mutant Na channels associated with myotonia and periodic paralysis. Biophysical J. *72*, 1204–1219. https://doi.org/10.1016/S0006-3495(97)78768-X.

Hilber, K., Sandtner, W., Kudlacek, O., Schreiner, B., Glaaser, I., Schütz, W., Fozzard, H.A., Dudley, S.C., and Todt, H. (2002). Interaction between fast and ultra-slow inactivation in the voltage-gated sodium channel. Does the inactivation gate stabilize the channel structure? J. Biol. Chem. *277*, 37105–37115. https://doi.org/10.1074/jbc.M205661200.

Hille, B. (2001). Ion Channels of Excitable Membranes (Sinauer Associates, Inc). https://doi.org/10.1007/978-94-009-7755-6_30.

Kalia, J., Milescu, M., Salvatierra, J., Wagner, J., Klint, J.K., King, G.F., Olivera, B.M., and Bosmans, F. (2015). From foe to friend: using animal toxins to investigate ion channel function. J. Mol. Biol. *427*, 158–175. https://doi.org/10.1016/j.jmb.2014.07.027.

Khodorov, B.I. (1985). Batrachotoxin as a tool to study voltage-sensitive sodium channels of excitable membranes. Prog. Biophys. Mol. Biol. *45*, 57–148. https://doi.org/10.1016/0079-6107(85)90005-7.

Khodorov, B.I., Yelin, E.A., Zaborovskaya, L.D., Maksudov, M.Z., Tikhomirova, O.B., and Leonov, V.N. (1992). Comparative analysis of the effects of synthetic derivatives of batrachotoxin on sodium currents in frog node of Ranvier. Cell Mol. Neurobiol. *12*, 59–81. https://doi.org/10.1007/BF00711639.

Lampert, A., O'Reilly, A.O., Reeh, P., and Leffler, A. (2010). Sodium channelopathies and pain. Pflugers Archiv Eur. J. Physiol. *460*, 249–263. https://doi.org/10.1007/s00424-009-0779-3.

Lenaeus, M.J., Gamal El-Din, T.M., Ing, C., Ramanadane, K., Pomès, R., Zheng, N., and Catterall, W.A. (2017). Structures of closed and open states of a voltage-gated sodium channel. Proc. Natl. Acad. Sci. U S A *114*, E3051–E3060. https://doi.org/10.1073/pnas.1700761114.

Li, H.L., Hadid, D., and Ragsdale, D.S. (2002). The batrachotoxin receptor on the voltage-gated sodium channel is guarded by the channel activation gate. Mol. Pharmacol. *61*, 905–912. https://doi.org/10.1124/mol.61.4.905.

Linford, N.J., Cantrell, A.R., Qu, Y., Scheuer, T., and Catterall, W.A. (1998). Interaction of batrachotoxin with the local anesthetic receptor site in transmembrane segment IVS6 of the voltage-gated sodium channel. Proc. Natl. Acad. Sci. U S A *95*, 13947–13952. https://doi.org/10.1073/pnas.95.23.13947.

Logan, M.M., Toma, T., Thomas-Tran, R., and Du Bois, J. (2016). Asymmetric synthesis of batrachotoxin: enantiomeric toxins show functional divergence against Na_V. Science *354*, 865–869. https://doi.org/10.1126/science.aag2981.

Lukowski, A.L., and Narayan, A.R.H. (2019). Natural voltage-gated sodium channel ligands: biosynthesis and biology. Chembiochem. *20*, 1231–1241. https://doi.org/10.1002/cbic.201800754.

Märki, F., and Witkop, B. (1963). The venom of the Colombian arrow poison frog *Phyllobates bicolor*. Experientia. *19*, 329–338. https://doi.org/10.1007/BF02152303.

Moran, O., Picollo, A., and Conti, F. (2003). Tonic and phasic guanidinium toxin-block of skeletal muscle Na channels expressed in mammalian cells. Biophysical J. *84*, 2999–3006. https://doi.org/10.1016/S0006-3495(03)70026-5.

Pan, X., et al. (2018). Structure of the human voltage-gated sodium channel $Na_V1.4$ in complex with β1. Science *362*, eaau2486. https://doi.org/10.1126/science.aau2486.

Patlak, J. (1991). Molecular kinetics of voltage-dependent Na^+ channels. Physiol. Rev. *71*, 1047–1080. https://doi.org/10.1152/physrev.1991.71.4.1047.

Payandeh, J. (2018). Progress in understanding slow inactivation speeds up. J. Gen. Physiol. *150*, 1235–1238. https://doi.org/10.1085/jgp.201812149.

Payandeh, J., and Minor Jr., D.L. (2015). Bacterial voltage-gated sodium channels ($BacNa_VS$) from the soil, sea, and salt lakes enlighten molecular mechanisms of electrical signaling and pharmacology in the brain and heart. J. Mol. Biol. *427*, 3–30. https://doi.org/10.1016/j.jmb.2014.08.010.

Peters, C.H., and Ruben, P.C. (2014). Introduction to sodium channels. In Voltage Gated Sodium Channels, P.C. Ruben, ed. (Springer), pp. 1–6. https://doi.org/10.1007/978-3-642-41588-3_1.

Ren, D., Navarro, B., Xu, H., Yue, L., Shi, Q., and Clapham, D.E. (2001). A prokaryotic voltage-gated sodium channel. Science *294*, 2372–2375.

Schow, S.R., Rossignol, D.P., Lund, A.E., and Schnee, M.E. (1997). Batrachotoxin binding site antagonists. Bioorg. Med. Chem. Lett. *7*, 181–186. https://doi.org/10.1016/S0960-894X(96)00596-3.

Shaya, D., Findeisen, F., Abderemane-Ali, F., Arrigoni, C., Wong, S., Nurva, S.R., Loussouarn, G., and Minor, D.L. (2014). Structure of a prokaryotic sodium channel pore reveals essential gating elements and an outer ion binding site common to eukaryotic channels. J. Mol. Biol. *426*, 467–483. https://doi.org/10.1016/j.jmb.2013.10.010.

Silva, J. (2014). Slow inactivation of Na^+ channels. In Voltage Gated Sodium Channels, P.C. Ruben, ed. (Springer), pp. 33–49.

Stevens, M., Peigneur, S., and Tytgat, J. (2011). Neurotoxins and their binding areas on voltage-gated sodium channels. Front. Pharmacol. *2*, 71. https://doi.org/10.3389/FPHAR.2011.00071.

Tanguy, J., and Yeh, J.Z. (1991). BTX modification of Na channels in squid axons. I. State dependence of BTX action. J. Gen. Physiol. *97*, 499–519. https://doi.org/10.1085/jgp.97.3.499.

Tikhonov, D.B., and Zhorov, B.S. (2005). Sodium channel activators: model of binding inside the pore and a possible mechanism of action. FEBS Lett. *579*, 4207–4212. https://doi.org/10.1016/j.febslet.2005.07.017.

Tokuyama, T., Daly, J., Witkop, B., Karle, I.L., and Karle, J. (1968). The structure of batrachotoxinin A, a novel steroidal alkaloid from the Colombian arrow poison frog, *Phyllobates aurotaenia*. J. Am. Chem. Soc. *90*, 1917–1918. https://doi.org/10.1021/ja01009a052.

Tokuyama, T., Daly, J., and Witkop, B. (1969). The structure of batrachotoxin, a steroidal alkaloid from the Colombian arrow poison frog, *Phyllobates aurotaenia*, and partial synthesis of batrachotoxin and its analogs and homologs. J. Am. Chem. Soc. *91*, 3931–3938. https://doi.org/10.1021/ja01042a042.

Toma, T., Logan, M.M., Menard, F., Devlin, A.S., and Du Bois, J. (2016). Inhibition of sodium ion channel function with truncated forms of batrachotoxin. ACS Chem. Neurosci. *7*, 1463–1468. https://doi.org/10.1021/acschemneuro.6b00212.

Vedantham, V., and Cannon, S.C. (1998). Slow inactivation does not affect movement of the fast inactivation gate in voltage-gated Na^+ channels. J. Gen. Physiol. *111*, 83–93. https://doi.org/10.1085/jgp.111.1.83.

Vilin, Y.Y., Fujimoto, E., and Ruben, P.C. (2001). A single residue differentiates between human cardiac and skeletal muscle Na^+ channel slow inactivation. Biophysical J. *80*, 2221–2230. https://doi.org/10.1016/S0006-3495(01)76195-4.

Wang, G.K., and Wang, S.Y. (1994). Modification of cloned brain Na^+ channels by batrachotoxin. Pflügers Archiv Eur. J. Physiol. *427*, 309–316. https://doi.org/10.1007/BF00374539.

Wang, S.Y., Nau, C., and Wang, G.K. (2000). Residues in Na^+ channel D3-S6 segment modulate both batrachotoxin and local anesthetic affinities. Biophysical J. *79*, 1379–1387. https://doi.org/10.1016/S0006-3495(00)76390-9.

Wang, S.-Y., Mitchell, J., Tikhonov, D.B., Zhorov, B.S., and Wang, G.K. (2006). How batrachotoxin modifies the sodium channel permeation pathway: computer modeling and site-directed mutagenesis. Mol. Pharmacol. *69*, 788–795. https://doi.org/10.1124/mol.105.018200.

Wang, S.Y., Bonner, K., Russell, C., and Wang, G.K. (2003). Tryptophan scanning of D1S6 and D4S6 C-termini in voltage-gated sodium channels. Biophysical J. *85*, 911–920. https://doi.org/10.1016/S0006-3495(03)74530-5.

Wang, S.Y., Tikhonov, D.B., Zhorov, B.S., Mitchell, J., and Wang, G.K. (2007). Serine-401 as a batrachotoxin- and local anesthetic-sensing residue in the human cardiac Na^+ channel. Pflugers Archiv Eur. J. Physiol. *454*, 277–287. https://doi.org/10.1007/s00424-006-0202-2.

Wang, S.Y., Barile, M., and Wang, G.K. (2001). Disparate role of Na^+ channel D2-S6 residues in batrachotoxin and local anesthetic action. Mol. Pharmacol. *59*, 1100–1107. https://doi.org/10.1124/mol.59.5.1100.

Wang, S.Y., and Wang, G.K. (1996). Slow inactivation of muscle μ1 Na^+ channels in permanently transfected mammalian cells. Pflugers Archiv Eur. J. Physiol. *432*, 692–699. https://doi.org/10.1007/s004240050187.

Wang, S.Y., and Wang, G.K. (1998). Point mutations in segment I-S6 render voltage-gated Na^+ channels resistant to batrachotoxin. Proc. Natl. Acad. Sci. U S A. *95*, 2653–2658. https://doi.org/10.1073/pnas.95.5.2653.

Wang, S.Y., and Wang, G.K. (1999). Batrachotoxin-resistant Na^+ channels derived from point mutations in transmembrane segment D4-S6. Biophysical J. *76*, 3141–3149. https://doi.org/10.1016/S0006-3495(99)77465-5.

Wang, S.Y., and Wang, G.K. (2003). Voltage-gated sodium channels as primary targets of diverse lipid-soluble neurotoxins. Cell Signal. *15*, 151–159. https://doi.org/10.1016/S0898-6568(02)00085-2.

Wang, S.Y., and Wang, G.K. (2017). Single rat muscle Na^+ channel mutation confers batrachotoxin autoresistance found in poison-dart frog *Phyllobates terribilis*. Proc. Natl. Acad. Sci. U S A. *114*, 10491–10496. https://doi.org/10.1073/pnas.1707873114.

Webb, J., Wu, F.F., and Cannon, S.C. (2009). Slow inactivation of the $Na_V1.4$ sodium channel in mammalian cells is impeded by co-expression of the β1 subunit. Pflugers Archiv. Eur. J. Physiol. *457*, 1253–1263. https://doi.org/10.1007/s00424-008-0600-8.

West, J.W., Patton, D.E., Scheuer, T., Wang, Y., Goldin, A.L., and Catterall, W.A. (1992). A cluster of hydrophobic amino acid residues required for fast Na^+-channel inactivation. Proc. Natl. Acad. Sci. U S A. *89*, 10910–10914. https://doi.org/10.1073/pnas.89.22.10910.

Yelin, E., Leonov, V., Tikhomirova, O., and Torgov, I. (2019). *Toxins as Tools in Neurochemistry: Proceedings of the Symposium Berlin (West), March 22–24, 1983*. In Toxins as Tools Neurochemistry, F. Hucho and Y. Ovchinnikov, eds. (De Gruyter), pp. 25–34.

Please cite this article in press as: MacKenzie et al., Differential effects of modified batrachotoxins on voltage-gated sodium channel fast and slow inactivation, Cell Chemical Biology (2021), https://doi.org/10.1016/j.chembiol.2021.12.003

STAR★METHODS

KEY RESOURCES TABLE

REAGENT or RESOURCE	SOURCE	IDENTIFIER
Chemicals, peptides, and recombinant proteins		
Dulbecco's Modified Eagle Medium (DMEM), high glucose	GIBCO, Grand Island, NY	Cat# 11965-118
Cosmic calf serum	HyClone, Logan, UT	Cat# SH3008703
Penicillin-streptomycin (10,000 U/mL)	GIBCO, Grand Island, NY	Cat# 15140122
Trypsin-EDTA 1X Solution	Invitrogen, Carlsbad, CA	Cat# 59417C
Batrachotoxin (BTX)	This study	N/A
Batrachotoxin-B (BTX-B)	This study	N/A
Batrachotoxin-^{c}Hx (BTX-^{c}Hx)	This study	N/A
Batrachotoxin-yne (BTX-yne)	This study	N/A
Experimental Models: Cell Lines		
Chinese hamster ovary (CHO) cells	Prof. Jon Sack, University of California, David, Department of Physiology and Membrane Biology	N/A
Human embryonic kidney (HEK293) cells	ATCC	Cat# CRL-1573
Recombinant DNA		
rSkM1 clone μ1-2 + pZem228-rNa$_V$1.4	Prof. S. Rock Levinson, University of Colorado, Department of Physiology and Biophysics	N/A
pcDNA3.1(+)-hNa$_V$1.5	Prof. Theodore Cummins, Indiana University, Department of Biology	N/A
pIRES-EGFP-NaVAe1	Shaya et al. (2014)	N/A
pTRACER-CMV2-NaVBh1	Ren et al. (2001)	N/A
Software and Algorithms		
IgorPro 6.37	Wavemetrics, Portland, OR	https://www.wavemetrics.com/software/igor-pro-637-installer
pClamp 10.4	Axon Instruments, Union City, CA	pClamp 10.3.2.1 download: https://support.moleculardevices.com/s/article/Axon-pCLAMP-10-Electrophysiology-Data-Acquisition-Analysis-Software-Download-Page? For pClamp 10.4, contact Molecular Devices through: https://support.moleculardevises.com/s/
Other		
Axopatch-200A Amplifier	Axon Instruments, Union City, CA	NA
Digidata 1322B Digitizer	Axon Instruments, Union City, CA	NA
Borosilicate glass micropipettes	Sutter Instruments, Novato, CA	Cat# BF150-110-10

RESOURCE AVAILABILITY

Lead contact

Further information and requests for resources and reagents should be directed to and will be fulfilled by the lead contact, Justin Du Bois (jdubois@stanford.edu).

Materials availability

Toxin derivatives generated in this study are limited in supply due to their difficulty of synthesis and toxicity, and require a material transfer agreement for distribution. Plasmids and cell lines can be requested by contacting the lead contact.

Please cite this article in press as: MacKenzie et al., Differential effects of modified batrachotoxins on voltage-gated sodium channel fast and slow inactivation, Cell Chemical Biology (2021), https://doi.org/10.1016/j.chembiol.2021.12.003

Data and code availability

- All data reported in this paper will be shared by the lead contact upon request.
- This paper does not report original code.
- Any additional information required to reanalyze the data reported in this paper is available from the lead contact upon request.

EXPERIMENTAL MODEL AND SUBJECT DETAILS

CHO and HEK cell cultures

Chinese hamster ovary (CHO) cells were obtained from Prof. Jon Sack (UC Davis) and were not further authenticated. Chinese hamster ovary and human embryonic kidney (HEK) cell cultures were prepared as described previously (Andresen and Du Bois, 2009; Shaya et al., 2014). Briefly, CHO cells were grown in DMEM (GIBCO, Grand Island, NY) supplemented with 10% cosmic calf serum (HyClone, Logan, UT) and 100 IU/mL penicillin/streptomycin (GIBCO). Cells were kept in a 5% carbon dioxide, 96% relative humidity incubator at 37°C and passaged every ~3 days. Passaging of cells was accomplished by aspiration of media, washing with phosphate-buffered saline, treatment with 1 mL trypsin-EDTA (0.05%, Invitrogen, Carlsbad, CA) for ~5 min until full dissociation of cells from the plate surface was observed and dilution with 4 mL of growth medium. Approximately 250 μL of this suspension was then diluted in 10 mL of growth medium in a new 10 cm plate. Human embryonic kidney cells (HEK293) were purchased from ATCC (CRL-1573) and were grown at 37°C under 5% CO_2, in a Dulbecco's modified Eagle's medium (DMEM) supplemented with 10% fetal bovine serum (FBS), 10% L-glutamine, and antibiotics (100 IU/mL penicillin and 100 mg/mL streptomycin) (University of California, San Francisco Cell Culture Facility). The sex of cell line is not determined.

METHOD DETAILS

Transient transfection of Na_V plasmids

Transfection with a pZem228 vector containing the full-length cDNA coding for the α-subunit of $rNa_V1.4$ was accomplished using the calcium phosphate precipitation method. Transfection with a pcDNA3.1(+) vector containing the full-length cDNA coding for the α-subunit of $hNa_V1.5$ was accomplished using Lipofectamine LTX. Transfection with a pIRES2-EGFP vector containing the full-length cDNA coding for Na_VAe1 or Na_VBh1 constructs was accomplished using Lipofectamine 2000. Cotransfection with EGFP was employed so that fluorescence of EGFP could be used as a marker of transfection efficiency.

Toxin quantification and storage

BTX derivatives were quantified by ^1H NMR spectroscopy on a 600 MHz Varian Inova spectrometer. 1,3-benzodioxole was employed as an internal standard. Spectra were acquired with a relaxation delay time (d1) of 20 s and an acquisition time (at) of 10 s. Quantitation was determined by comparison of the integrations for the toxin and the internal standard of a known concentration. Toxin stock solutions prepared in dimethylsulfoxide (4 mM) were kept at −20°C and diluted with external solution before recording.

Electrophysiology

Sodium currents were measured using the patch-clamp technique in the whole-cell configuration with an Axopatch-200b amplifier (Axon Instruments, Union City, CA), as previously described by Moran and coworkers (Moran et al., 2003). Borosilicate glass micropipettes (Sutter Instruments, Novato, CA) were fire-polished to a tip diameter yielding a resistance of 1.2–4.5 MΩ in the working solutions. The micropipette was filled with 40 mM NaF, 1 mM EDTA, 20 mM HEPES, 125 mM CsCl. The external solution had the following composition: 160 mM NaCl, 2 mM $CaCl_2$, 20 mM HEPES. The pH of the solutions was adjusted to pH 7.4 with 50 wt% aqueous CsOH.

The output of the patch-clamp amplifier was filtered with a built-in low-pass, four-pole Bessel filter having a cutoff frequency of 10 kHz and sampled at 100 kHz. The membrane was kept at a holding potential of −100 mV. Pulse stimulation and data acquisition used 16-bit D-A and A-D converters (Axon Instruments Digidata 1322A) controlled with the pClamp software (Axon Instruments). Leak currents were subtracted using a standard P/4 protocol of the same polarity. Access resistance was always <4 MΩ and the cell capacitance was between 4 and 20 pF, as measured by the compensating circuit of the feedback amplifier. Peak currents were generally between 1 and 5 nA. The series resistance was typically compensated 80%. All measurements were done at ambient temperature (20–22°C). Recordings were made at least 5 min after establishing the whole-cell and voltage-clamp configuration to allow for stabilization of the voltage-dependent properties of the channels.

Cells were modified by toxin after stabilization of whole-cell voltage parameters and control measurements. 0.5 mL of toxin solution was applied over 60 s. Toxin binding was promoted via 2,000 pulses to 0 mV from a hold potential of −100 mV (2 Hz cycling) before measurements were performed.

Chemistry: general experimental

Unless stated otherwise, all reactions were performed at ambient temperature in flame-dried or oven-dried glassware under an argon or nitrogen atmosphere using dry, deoxygenated solvents (distilled or passed over a column of activated alumina). Air- and moisture-sensitive liquids and solutions were transferred via syringe or stainless steel cannula. Organic solutions were concentrated under reduced pressure (~15 Torr) by rotary evaporation. Commercially available reagents were used as received. Triethylamine was

distilled from calcium hydride immediately prior to use. Reactions requiring external heat were modulated to specified temperatures using an IKAmag temperature controller. Thin-layer chromatography (TLC) was performed using E. Merck silica gel 60 F254 pre-coated plates (250 nm) and visualized by UV fluorescence quenching, potassium permanganate, aqueous ceric ammonium molybdate, or *p*-anisaldehyde staining. Silicycle SiliaFlash P60 Academic Silica gel (particle size 40–63 nm) was used for flash chromatography. In select cases as indicated, NH_4OH pre-treated silica gel was used for chromatographic separation as described previously (Logan, 2016). Briefly, preparation of NH_4OH pre-treated silica gel was accomplished by slurrying silica gel with concentrated aqueous NH_4OH in a large crystallization dish, followed by evaporation of water by heating at 50°C on a hot plate overnight.

^1H and ^{13}C NMR spectra were recorded on a Varian Inova 400 (400 MHz and 100 MHz, respectively), a Varian Inova 500 (500 MHz and 125 MHz, respectively), or a Varian Inova 600 (600 MHz and 150 MHz, respectively) and are reported in terms of chemical shift relative to residual $CHCl_3$ (in $CDCl_3$, δ 7.26 and δ 77.16, respectively) or C_6H_6 (in C_6D_6, δ 7.16 and δ 128.39, respectively). Data for ^1H NMR spectra are reported as follows: chemical shift (δ, ppm), multiplicity (s, singlet; d: doublet; t, triplet; q, quartet; m, multiplet), coupling constant (Hz), integration. Data for ^{13}C are reported in terms of chemical shift (δ, ppm). Infrared spectra were recorded as thin films using NaCl salt plates on a Thermo-Nicolet 300 FT-IR and are reported in frequency of absorption. High-resolution mass spectra were obtained from the Vincent Coates Foundation Mass Spectrometry Laboratory at Stanford University. Samples were analyzed by liquid chromatography-electrospray ionization mass spectrometry on a Waters Acquity UPLC and Thermo Fisher Exactive Mass Spectrometer scanning m/z 100-1,000. The LC mobile phase was 100% methanol and the flow rate was 0.175 mL/min.

Caution

Batrachotoxin (BTX) and synthetic derivatives thereof are (or may be) extremely potent neurotoxins (LD_{50} = 1–2 μg/kg; mouse, subcutaneous) (Tokuyama et al., 1969) and should be handled with great care. The compounds are skin permeable and may cause paralysis or death if contact with skin occurs. Proper personal protective equipment should be worn at all times.

Synthetic experimental procedures

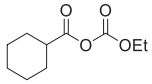

Cyclohexanecarboxylic (ethyl carbonic) anhydride

To an ice-cold solution of cyclohexane-carboxylic acid (548 mg, 4.27 mmol) in 21 mL of benzene was added sequentially Et_3N (410 μL, 4.27 mmol) and ethyl chloroformate (600 μL, 4.27 mmol). The solution was stirred at 0°C for 30 min. Following this time, the reaction mixture was transferred to a separatory funnel with 30 mL of Et_2O and 30 mL of 1.0 M aqueous NaOH. The organic layer was collected and the aqueous layer was extracted with 3 x 50 mL of Et_2O. The combined organic extracts were dried over $MgSO_4$, filtered, and concentrated under reduced pressure to a yellow oil. Purification of this material by chromatography on silica gel (20% Et_2O/hexanes) afforded cyclohexanecarboxylic (ethyl carbonic) anhydride as a clear oil (692 mg, 81%).

^1H NMR (500 MHz, $CDCl_3$) δ 4.31 (q, J = 7.1 Hz, 2H), 2.43 (tt, J = 11.3, 3.7 Hz, 1H), 1.98 (d, J = 13.2 Hz, 2H), 1.81–1.75 (m, 2H), 1.68–1.61 (m, 2H), 1.56–1.43 (m, 2H), 1.36 (t, J = 7.2 Hz, 3H), 1.32–1.19 (m, 2H) ppm

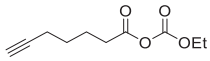

Hept-6-ynecarboxylic (ethyl carbonic) anhydride

To an ice-cold solution of hept-6-yne carboxylic acid (299 mg, 2.37 mmol) in 12 mL of benzene was added sequentially Et_3N (230 μL, 2.37 mmol) and ethyl chloroformate (330 μL, 2.37 mmol). The solution was stirred at 0°C for 30 min. Following this time, the reaction mixture was transferred to a separatory funnel with 30 mL of Et_2O and 30 mL of 1.0 M aqueous NaOH. The organic layer was collected and the aqueous layer was extracted with 3 x 50 mL of Et_2O. The combined organic extracts were dried over $MgSO_4$, filtered, and concentrated under reduced pressure to a yellow oil. Purification of this material by chromatography on silica gel (10% EtOAC/hexanes) afforded the desired product as a clear oil (368 mg, 78%).

TLC R_f = 0.55 (25% EtOAc/hexanes)

^1H NMR (400 MHz, $CDCl_3$) δ 4.32 (q, J = 7.2 Hz, 2H), 2.50 (t, J = 7.4 Hz, 2H), 2.23 (td, J = 7.0, 2.6 Hz, 2H), 1.96 (t, J = 2.7 Hz, 1H), 1.81 (dt, J = 15.3, 7.5 Hz, 2H), 1.61 (dt, 14.5, 7.1 Hz, 2H), 1.36 (t, 7.2 Hz, 3H) ppm.

^{13}C NMR (100 MHz, $CDCl_3$) δ 167.8, 149.2, 83.7, 69.0, 65.8, 33.8, 27.6, 23.4, 18.2, 14.1 ppm.

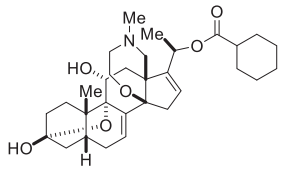

BTX-^{c}Hx

To a solution of batrachotoxinin A (1.6 mg, 3.8 μmol) in 2.0 mL of anhydrous benzene were sequentially added Et_3N (150 μL, 1.1 mmol, 289 equiv) and cyclohexanecarboxylic (ethyl carbonic) anhydride (10 mg, 49.9 μmol, 13.1 equiv). The reaction mixture was stirred at 45°C for 18 h. Following this time, all volatiles were removed under reduced pressure to give a pale yellow residue. This material was transferred to a 16 × 125 mm test tube with 4 mL of $CHCl_3$. The solution was cooled in an ice bath and 4.0 mL of ice-cold 0.1 M aqueous HCl was added slowly. With the aid of a glass pipet, the layers were mixed, the $CHCl_3$ layer was carefully removed, and the aqueous layer was extracted with 1 x 4.0 mL of $CHCl_3$. The combined organic fractions were discarded. The pH of the aqueous layer was then adjusted to 10 with 2 mL of 1.0 M aqueous NH_4OH, and the solution was extracted with 3 x 4 mL of $CHCl_3$. The combined organic fractions were dried over Na_2SO_4, filtered, and concentrated under reduced pressure to a colorless residue. Purification of this material by chromatography on NH_4OH pre-treated silica gel (gradient elution: 30% EtOAc/pentane → 70% EtOAc/pentane with 1% v/v Et_3N) afforded BTX-^{c}Hx as a white solid (1.3 mg, 65%).

TLC R_f = 0.41 (10% MeOH/CH_2Cl_2 on NH_4OH pre-treated silica gel plates)

^{1}H NMR (600 MHz, $CDCl_3$) δ 6.18-6.14 (m, 1H), 5.82 (s, 1H), 5.67 (q, J = 6.5 Hz, 1H), 3.70 (td, J = 10.7, 3.6 Hz, 1H), 3.64 (dt, J = 13.4, 4.5 Hz, 1H), 3.52 (ddd, J = 13.2, 9.0, 4.0 Hz, 1H), 3.17 (d, J = 17.6 Hz, 1H), 2.93–2.86 (m, 1H), 2.79 (d, J = 14.0 Hz, 1H), 2.59 (d, J = 13.2 Hz, 1H), 2.53 (d, J = 14.1, 1H), 2.44 (ddd, J = 18.9, 4.7, 2.2 Hz, 1H), 2.34 (s, 3H), 2.31–2.19 (m, 2H), 2.16 (dd, J = 13.0, 10.6 Hz, 3H), 1.92 (dd, J = 13.8, 11.2 Hz, 4H), 1.82 (td, J = 12.6, 3.9 Hz, 1H), 1.77 (s, 1H), 1.75 (s, 3H), 1.64 (q, J = 17.0, 14.5 Hz, 4H), 1.54 (s, 3H), 1.48 (dd, J = 9.3, 4.0 Hz, 1H), 1.41 (d, J = 6.4 Hz, 3H), 1.38–1.30 (m, 1H), 1.07 (s, 1H), 0.90 (s, 3H) ppm

HRMS (ESI$^+$) calcd for $C_{31}H_{45}NO_6$ 527.3247 found 528.3313 ($M+H^+$)

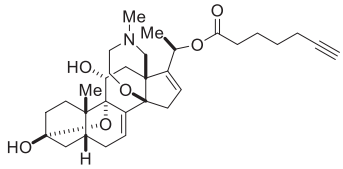

BTX-yne

To a solution of batrachotoxinin A (1.3 mg, 3.1 μmol) in 2.0 mL of anhydrous benzene were sequentially added Et_3N (100 μL, 730 μmol, 235 equiv) and hept-6-ynecarboxylic (ethyl carbonic) anhydride (10 mg, 50.4 μmol, 16.3 equiv). The reaction mixture was stirred at 45°C for 18 h. Following this time, all volatiles were removed under reduced pressure to give a pale yellow residue. This material was transferred to a 16 × 125 mm test tube with 4 mL of $CHCl_3$. The solution was cooled in an ice bath and 4.0 mL of ice-cold 0.1 M aqueous HCl was added slowly. With the aid of a glass pipet, the layers were mixed, the $CHCl_3$ layer was carefully removed, and the aqueous layer was extracted with 1 x 4.0 mL of $CHCl_3$. The combined organic fractions were discarded. The pH of the aqueous layer was then adjusted to 10 with 2 mL of 1.0 M aqueous NH_4OH, and the solution was extracted with 3 x 4 mL of $CHCl_3$. The combined organic fractions were dried over Na_2SO_4, filtered, and concentrated under reduced pressure to a colorless residue. Purification of this material by chromatography on NH_4OH pre-treated silica gel (gradient elution: 30% EtOAc/pentane → 70% EtOAc/pentane with 1% v/v Et_3N) afforded BTX-yne as a white solid (0.9 mg, 56%)

TLC R_f = 0.39 (25% pentane/EtOAc with 10% v/v Et_3N)

^{1}H NMR (600 MHz, $CDCl_3$) δ 6.17 (d, J = 5.0 Hz, 1H), 5.83 (s, 1H), 5.65 (q, J = 6.4 Hz, 1H), 3.74–3.62 (m, 2H), 3.52 (ddd, J = 13.0, 8.5, 4.0 Hz, 1H), 3.18 (d, J = 17.8 Hz, 1H), 2.87 (d, J = 8.5 Hz, 1H), 2.79 (d, J = 13.9 Hz, 1H), 2.55 (dd, J = 31.9, 13.4 Hz, 2H), 2.44 (ddd, J = 18.7, 4.8, 2.2 Hz, 1H), 2.36–2.29 (m, 4H), 2.27 (s, 1H), 2.23 (td, J = 7.1, 2.8 Hz, 3H), 2.20–2.13 (m, 3H), 2.00 (t, J = 2.7 Hz, 1H), 1.98–1.88 (m, 2H), 1.85–1.70 (m, 5H), 1.68–1.60 (m, 2H), 1.60–1.54 (m, 4H), 1.45–1.41 (m, 3H), 0.89 (s, 3H) ppm.

^{13}C NMR (150 MHz, C_6D_6) 173.6, 152.8, 142.3, 127.1, 124.3, 95.5, 87.9, 84.0, 82.1, 79.1, 69.3, 67.7, 67.5, 67.1, 60.8, 60.3, 59.6, 57.5, 47.3, 47.1, 40.5, 37.0, 34.4, 32.5, 28.1, 24.3, 23.0, 21.8, 19.6, 19.3, 18.2 ppm.

IR (thin film) ν 3308 (br), 2927, 1722, 1463, 1372, 1261 cm^{-1}

HRMS (ESI$^+$) calcd for $C_{31}H_{43}NO_6$ 525.3090 found 526.3155 ($M+H^+$)

QUANTIFICATION AND STATISTICAL ANALYSIS

Data were analyzed using the Igor Pro 6.37 environment (Wavemetrics). Fit of data is presented as mean ± SD. All experiments are presented as mean ± SEM for $n \geq 3$ independent measurements. All statistical details can be found in figure legends and/or table captions.